cAMP-activated Ca^{2+} signaling is required for CFTR-mediated serous cell fluid secretion in porcine and human airways

Robert J. Lee[1] and J. Kevin Foskett[1,2]

[1]Department of Physiology and [2]Department of Cell and Developmental Biology, University of Pennsylvania, Philadelphia, Pennsylvania, USA.

Cystic fibrosis (CF), which is caused by mutations in CFTR, affects many tissues, including the lung. Submucosal gland serous acinar cells are primary sites of fluid secretion and CFTR expression in the lung. Absence of CFTR in these cells may contribute to CF lung pathogenesis by disrupting fluid secretion. Here, we have isolated primary serous acinar cells from wild-type and *CFTR*$^{-/-}$ pigs and humans without CF to investigate the cellular mechanisms and regulation of fluid secretion by optical imaging. Porcine and human serous cells secrete fluid in response to vasoactive intestinal polypeptide (VIP) and other agents that raise intracellular cAMP levels; here, we have demonstrated that this requires CFTR and a cAMP-dependent rise in intracellular Ca^{2+} concentration ($[Ca^{2+}]_i$). Importantly, cAMP induced the release of Ca^{2+} from $InsP_3$-sensitive Ca^{2+} stores also responsive to cAMP-independent agonists such as cholinergic, histaminergic, and purinergic agonists that stimulate CFTR-independent fluid secretion. This provides two types of synergism that strongly potentiated cAMP-mediated fluid secretion but differed in their CFTR dependencies. First, CFTR-dependent secretion was strongly potentiated by low VIP and carbachol concentrations that individually were unable to stimulate secretion. Second, higher VIP concentrations more strongly potentiated the $[Ca^{2+}]_i$ responses, enabling ineffectual levels of cholinergic stimulation to strongly activate CFTR-independent fluid secretion. These results identify important molecular mechanisms of cAMP-dependent secretion, including a requirement for Ca^{2+} signaling, and suggest new therapeutic approaches to correct defective submucosal gland secretion in CF.

Introduction

Submucosal exocrine glands secrete much of the fluid and mucus that hydrate the surfaces of cartilaginous airways in the lungs (1). Serous acini are thought to be the primary site of fluid secretion, although the geometrical complexity and numerous cell types present in the glands have impeded investigations of the molecular mechanisms generating and regulating the volume and composition of the secreted fluid. Serous acinar cells express the CFTR anion channel (2–4), which may play a role in fluid secretion elicited by agonists that raise intracellular [cAMP] ($[cAMP]_i$; refs. 5–8). Absence of this fluid secretion mechanism in cystic fibrosis (CF) may contribute to CF lung pathogenesis (9).

Vasoactive intestinal polypeptide (VIP) belongs to the secretin family of peptides, which usually signal via $G\alpha_s$-stimulated adenylyl cyclase–mediated elevation of $[cAMP]_i$ (10). VIP receptors are expressed in submucosal gland acini, which lie in close proximity to VIP-containing neurons (reviewed in ref. 11). VIP elevates $[cAMP]_i$ in serous and mucous cells of ferret tracheal submucosal glands (12) and stimulates airway glycoprotein secretion (13–15) and CFTR-dependent fluid secretion from intact human, porcine, and murine submucosal glands (5–8). These secretory responses are mimicked by the adenylyl cyclase–activating compound forskolin (5, 7, 8, 16). Gland fluid secretion is also elicited by cholinergic agonists, including carbachol (CCh). Strong cholinergic stimulation activates CFTR-independent secretion in human, porcine, and murine glands (6–8). In porcine and murine serous cells, CCh-induced secretion is intracellular Ca^{2+} dependent and mediated in the same CFTR-expressing cells by a different Cl^- channel, likely the Ca^{2+}-activated Cl^- channel (CaCC) Ano1 (TMEM16A; refs. 3, 4, and 17). Smaller secretory responses evoked by submaximal cholinergic stimulation are potentiated by low VIP concentrations (10–100 nM) that are insufficient themselves to activate robust secretion in both human and pig glands (18). Interestingly, this potentiation is CFTR dependent, suggesting that CFTR also plays a role in responses to submaximal cholinergic stimulation, but the molecular and cellular details of this synergism are not understood.

Despite their potential importance to CF pathology, the molecular mechanisms involved in serous acinar cell fluid secretion remain poorly defined. Here, we have examined cAMP-induced fluid secretion in porcine and human submucosal gland serous cells isolated from WT and *CFTR* KO (*CFTR*$^{-/-}$) pigs and non-CF humans. Our results demonstrate that VIP stimulates fluid secretion by a CFTR-dependent mechanism requiring a concomitant cAMP-induced release of Ca^{2+} from inositol trisphosphate–sensitive ($InsP_3$-sensitive) intracellular stores and a rise of intracellular $[Ca^{2+}]$ ($[Ca^{2+}]_i$). CFTR provides the secretory Cl^- permeability, whereas the rise of $[Ca^{2+}]_i$ is necessary to activate plasma membrane K^+ permeabilities. Importantly, $[Ca^{2+}]_i$ responses to weak CCh stimulation that are insufficient to stimulate secretion are markedly potentiated by strong cAMP stimulation, resulting in robust cAMP-mediated CFTR-independent secretion and suggesting novel strategies to bypass the CFTR requirement for cAMP-mediated fluid secretion.

Results

VIP activation of porcine bronchial submucosal gland serous cell secretion requires cAMP-activated Ca^{2+} signaling. Stimulation of isolated por-

Conflict of interest: The authors have declared that no conflict of interest exists.

Citation for this article: *J Clin Invest.* 2010;120(9):3137–3148. doi:10.1172/JCI42992.

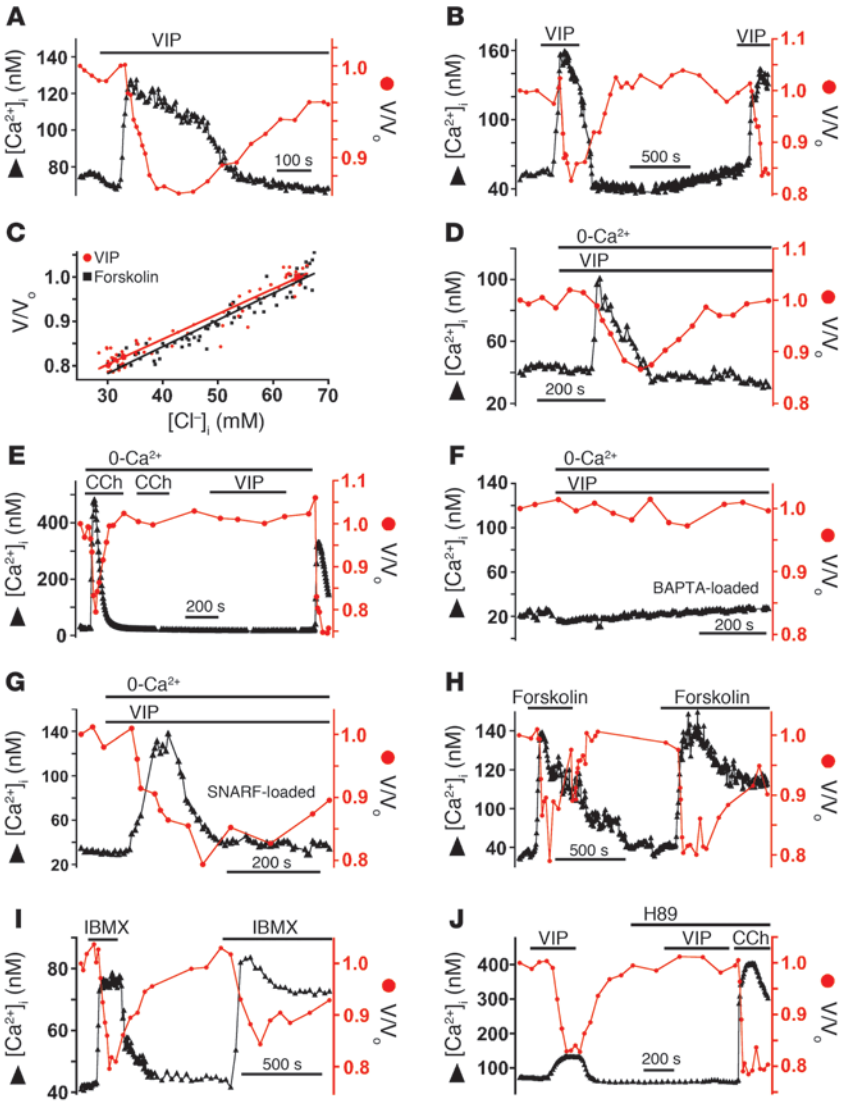

Figure 1

VIP-stimulated porcine serous cell secretion requires cAMP-dependent Ca^{2+} signaling. (**A** and **B**) Representative traces showing 1 μM VIP-evoked $[Ca^{2+}]_i$ (triangles) and cell volume (circles; normalized to volume at time = 0 [V/V_o]) responses, which were reproducible (**B**). (**C**) Cell volume and $[Cl^-]_i$ were linearly correlated during VIP and forskolin exposure. 75 points plotted from 6 forskolin experiments (squares) and 82 points from 5 VIP experiments (circles). SPQ fluorescence changes (Supplemental Figure 1) converted to $[Cl^-]_i$ as described (3, 38). (**D**) Representative trace showing transient $[Ca^{2+}]_i$ elevation and shrinkage during VIP exposure in 0-$Ca^{2+}{}_o$. (**E**–**F**) After depletion of Ca^{2+} stores by repeated stimulation with 100 μM CCh in 0-$Ca^{2+}{}_o$ (**E**) or in BAPTA-loaded $[Ca^{2+}]_i$-buffered cells (**F**), VIP exposure in 0-Ca^{2+} resulted in neither $[Ca^{2+}]_i$ elevation nor shrinkage. (**G**) Cells loaded with SNARF-5F-AM (which does not chelate $[Ca^{2+}]_i$) exhibited normal $[Ca^{2+}]_i$ elevation (134 ± 17 nM) and shrinkage (17% ± 2% within 130 ± 22 s; $n = 4$; NS compared with VIP/0-Ca^{2+} stimulation as in Figure 1D). (**H**) Forskolin (10 μM) caused concomitant shrinkage (15% ± 2%; $n = 6$) and $[Ca^{2+}]_i$ elevation (130 ± 11 nM; $n = 10$; values NS compared with 1 μM VIP). (**I**) IMBX (250 μM) caused simultaneous $[Ca^{2+}]_i$ elevation (97 ± 10 nM; $n = 3$) and shrinkage (18% ± 2%; values NS compared with 1 μM VIP). (**J**) VIP-stimulated responses were abolished by H89; responses to 1 μM CCh remained intact.

cine bronchial serous acinar cells with 1 μM VIP caused a 15% ± 2% cell shrinkage (within 107 ± 29 s; $n = 7$) that reversed upon washout (Figure 1, A and B). Similar cell volume changes during cholinergic stimulation result from changes in cell solute content associated with activation of ion channels and transporters that mediate fluid secretion (3, 4). Shrinkage is caused by activation of apical membrane Cl^- and/or basolateral membrane K^+ channels, resulting in KCl efflux; swelling is caused by activities of Na^+-dependent Cl^- uptake pathways in the basolateral membrane (3, 4). In agreement, VIP-induced volume changes were temporally and quantitatively paralleled by changes in $[Cl^-]_i$ (Figure 1C and Supplemental Figure 1; supplemental material available online with this article; doi:10.1172/JCI42992DS1). Furthermore, swelling was inhibited by the $Na^+K^+2Cl^-$ cotransporter (NKCC) inhibitor bumetanide and the Na^+/H^+ exchanger (NHE) inhibitor dimethyl amiloride (Supplemental Figure 2), indicating that NKCC1 and paired NHE and Cl^-/HCO_3^- (anion) exchange (AE) mediate solute uptake, as shown for cholinergic-activated secretion by these cells (4). Thus, VIP-induced cell volume changes report alterations in cell solute content reflecting changes in the secretory state of these cells (4). VIP-evoked shrinkage reflects solute efflux occurring upon activation of fluid secretion, while swelling reflects accumulation of solute via transporters that sustain secretion.

During cholinergic stimulation, cell volume closely tracks agonist-induced changes in $[Ca^{2+}]_i$ (4). Surprisingly, VIP consistently caused a small rise in $[Ca^{2+}]_i$, from 45 ± 7 nM at rest to a peak of 101 ± 12 nM ($n = 7$), that was temporally correlated with cell shrinkage (Figure 1, A and B). Furthermore, relaxation of $[Ca^{2+}]_i$ toward resting levels was associated with cell swelling back to resting volume. The strong temporal correlation between dynamic $[Ca^{2+}]_i$ and volume changes was unexpected. While VIP has been linked to Ca^{2+} signaling in some cell types (10, 19–25), the mechanisms involved are unclear, and VIP has been assumed to activate airway gland fluid secretion solely by raising $[cAMP]_i$. A direct role for Ca^{2+} in VIP-evoked secretion has not been considered.

Stimulation with 1 μM VIP in the absence of extracellular Ca^{2+} (0-$Ca^{2+}{}_o$) elicited transient $[Ca^{2+}]_i$ and shrinkage responses (Figure 1D; $n = 7$). Peak $[Ca^{2+}]_i$ was similar in cells stimulated in the absence or presence of $Ca^{2+}{}_o$ (98 ± 5 nM in 0-$Ca^{2+}{}_o$ vs. 101 ± 12 nM with $Ca^{2+}{}_o$; NS), indicating that VIP mobilizes Ca^{2+} from intracellular stores, with sustained $[Ca^{2+}]_i$ responses requiring extracellular Ca^{2+} influx. When cells were stimulated with 100 μM CCh in 0-$Ca^{2+}{}_o$

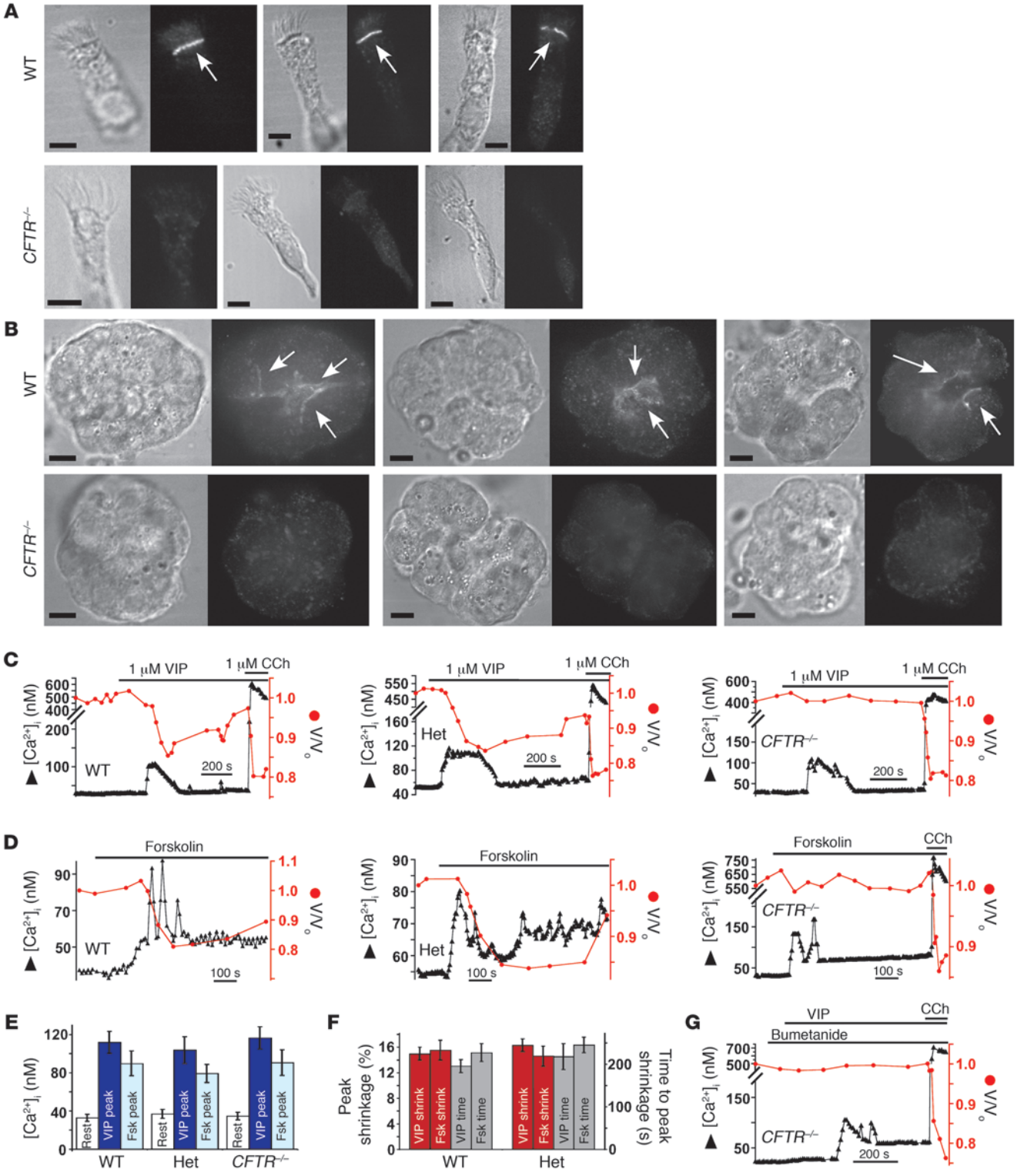

Figure 2

VIP-activated porcine serous cell secretion requires CFTR. (**A**–**B**) Micrographs showing CFTR immunostaining in WT and *CFTR*$^{-/-}$ porcine tracheal ciliated epithelial cells (**A**) and serous acini (**B**). Arrows indicate apical membrane immunofluorescence observed only in WT cells. Scale bars: 5 μm. (**C** and **D**) Representative traces showing VIP-evoked (**C**) and forskolin-evoked (**D**) volume and $[Ca^{2+}]_i$ responses in WT, Het, and *CFTR*$^{-/-}$ cells. (**E**) Summary of resting and peak $[Ca^{2+}]_i$. (**F**) Summary of shrinkage (red) and time to shrinkage (gray) in WT and Het cells. VIP-stimulated shrinkage was 15% ± 1% within 196 ± 15 s (WT; $n = 6$) and 16% ± 1% within 218 ± 31 s (Het.; $n = 6$; all values NS). Forskolin-stimulated shrinkage was 16% ± 2% within 228 ± 21 s (WT; $n = 14$) and 15% ± 2% within 245 ± 18 s (Het.; $n = 8$; all values NS). (**G**) Bumetanide (100 μM) did not enhance VIP-evoked shrinkage in *CFTR*$^{-/-}$ cells.

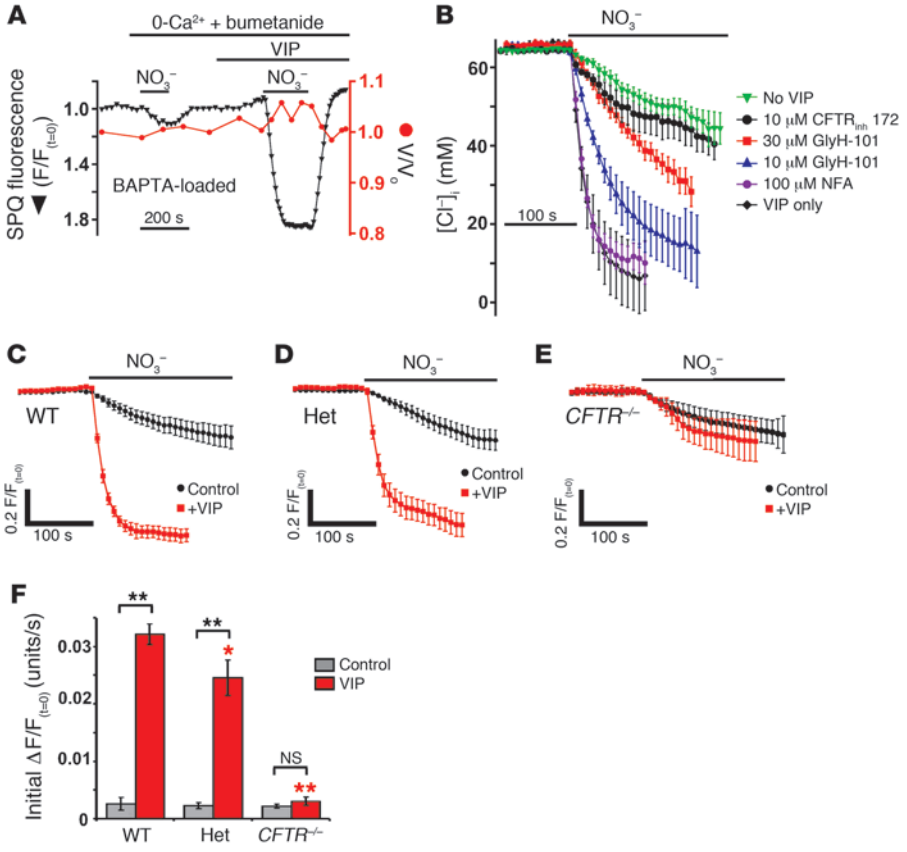

Figure 3

VIP-induced $[Ca^{2+}]_i$ elevation is not required for activation of CFTR-dependent anion permeability in porcine serous cells. (**A**) SPQ fluorescence (black inverted triangles) during substitution of Cl^-_o with $NO_3^-_o$ before and during exposure to 1 μM VIP in presence of 100 μM bumetanide and 0-CO_2/HCO_3^- in 0-Ca^{2+}_o, BAPTA-loaded conditions that inhibit shrinkage. (**B**) Average responses to NO_3^- substitution (raw traces shown in Supplemental Figure 5) in absence of VIP (n = 7) or after 180–200 s exposure to 1 μM VIP (n = 8) ± 100 μM NFA (n = 5), 10 μM GlyH-101 (n = 5), 30 μM GlyH-101 (n = 4), or 10 μM $CFTR_{inh}172$ (n = 9). Fluorescence normalized to that at time = 0 ($F/F_{(t=0)}$) and converted to $[Cl^-]_i$ (4) before averaging. (**C**–**E**) Cl^- permeability measured as above in WT (**C**), Het (**D**), or *CFTR*$^{-/-}$ (**E**) tracheal cells either unstimulated or stimulated for 180–200 s with 1 μM VIP. SPQ fluorescence plotted inversely (downward deflection = increase in SPQ fluorescence = decrease in $[Cl^-]_i$). (**F**) Initial rates of SPQ fluorescence increase in unstimulated (control) and 1 μM VIP-stimulated WT (n = 12), Het (n = 7), and *CFTR*$^{-/-}$ (n = 8) cells. Red asterisks indicate significance of VIP-stimulated rates (red bars) compared with WT (Dunnett's test). Black asterisks indicate significance between control and VIP-stimulated rates (gray versus red bar; Student's t test) within each genotype. *P < 0.05; **P < 0.01.

to deplete intracellular Ca^{2+} stores before stimulation with VIP in 0-Ca^{2+}_o, both $[Ca^{2+}]_i$ and secretory responses to VIP were eliminated (Figure 1E). The same cells robustly shrank upon reintroduction of Ca^{2+}_o and subsequent $[Ca^{2+}]_i$ elevation (Figure 1E). VIP-evoked $[Ca^{2+}]_i$ and shrinkage responses in 0-Ca^{2+}_o were also eliminated in cells loaded with the Ca^{2+} chelator BAPTA (10 μM for 1 hour as in ref. 4; Figure 1F). Responses remained intact in control cells (Figure 1G), suggesting that VIP-evoked shrinkage is absent in BAPTA-loaded cells because of the lack of Ca^{2+} response and not generalized toxic effects of AM-ester loading. Thus, VIP-induced $[Ca^{2+}]_i$ signals are required for VIP-mediated serous cell fluid secretion.

To further define the role of cAMP in serous cell secretion, $[cAMP]_i$ was raised independently of receptor activation. Forskolin (10 μM) elicited shrinkage with magnitude and kinetics similar to those induced by 1 μM VIP that, importantly, also coincided with a similar simultaneous elevation of $[Ca^{2+}]_i$ (Figure 1H). Forskolin-induced volume changes paralleled changes in $[Cl^-]_i$ as with VIP (Figure 1C and Supplemental Figure 1). The phosphodiesterase inhibitor 3-isobutyl-1-methylxanthine (IBMX; 250 μM) also caused comparable shrinkage correlated with $[Ca^{2+}]_i$ elevation (Figure 1I). No additive effects were observed between 250 μM IBMX and 1 μM VIP (discussed below), suggesting they both signal through cAMP, likely involving PKA. In agreement, the PKA inhibitor H89 completely abolished VIP-induced $[Ca^{2+}]_i$ elevation and shrinkage but had no effect on subsequent CCh-evoked responses (Figure 1J).

VIP-activated secretion requires CFTR. Fluid secretion elicited by VIP by intact glands requires CFTR. It has been assumed that VIP stimulates secretion solely by PKA-mediated CFTR activation. However, our results suggest that serous cell secretion also requires cAMP-induced $[Ca^{2+}]_i$ signaling. Cholinergic stimulation of serous cell secretion similarly requires Ca^{2+} signaling, but it is CFTR independent (3, 4, 17). Nevertheless, the CFTR inhibitors GlyH-101 (26) and $CFTR_{inh}172$ (27), which do not affect cholinergic-induced secretion (3, 4), each inhibited VIP- or forskolin-activated shrinkage (Supplemental Figure 3). To examine the role of CFTR more directly, we isolated cells from neonatal porcine *CFTR*$^{+/+}$ WT, and *CFTR*$^{+/-}$ heterozygote (Het), and *CFTR*$^{-/-}$ knockout tracheal submucosal glands (28). *CFTR*$^{-/-}$ piglets develop significant CF-like lung disease within months after birth (29), but neonatal *CFTR*$^{-/-}$ piglets are free of airway pathology (28, 29), providing a model to directly compare *CFTR*$^{-/-}$ and isogenic WT littermates and examine effects of lack of CFTR in the absence of secondary pathology. Apical CFTR immunofluorescence was detected in ciliated epithelial cells (Figure 2A) and serous acini (Figure 2B) from WT but not *CFTR*$^{-/-}$ tracheae. Serous cells from WT and Het piglets exhibited VIP- (Figure 2C) and forskolin-evoked (Figure 2D) $[Ca^{2+}]_i$ signals and shrinkage (summarized in Figure 2, E and F) that were identical to each other and nearly identical to those observed in adult WT bronchial serous cells. Despite identical $[Ca^{2+}]_i$ responses (Figure 2, E and F), *CFTR*$^{-/-}$ cells did not shrink in response to either VIP (Figure 2C) or forskolin (Figure 2D), even in the presence of bumetanide to prevent compensatory solute influx (Figure 2G). These results establish an essential requirement for CFTR in cAMP-activated serous cell secretion. In contrast, *CFTR*$^{-/-}$ and WT cells exhibited identical secretory responses to CCh (250 nM to 10 μM; Supplemental Figure 4).

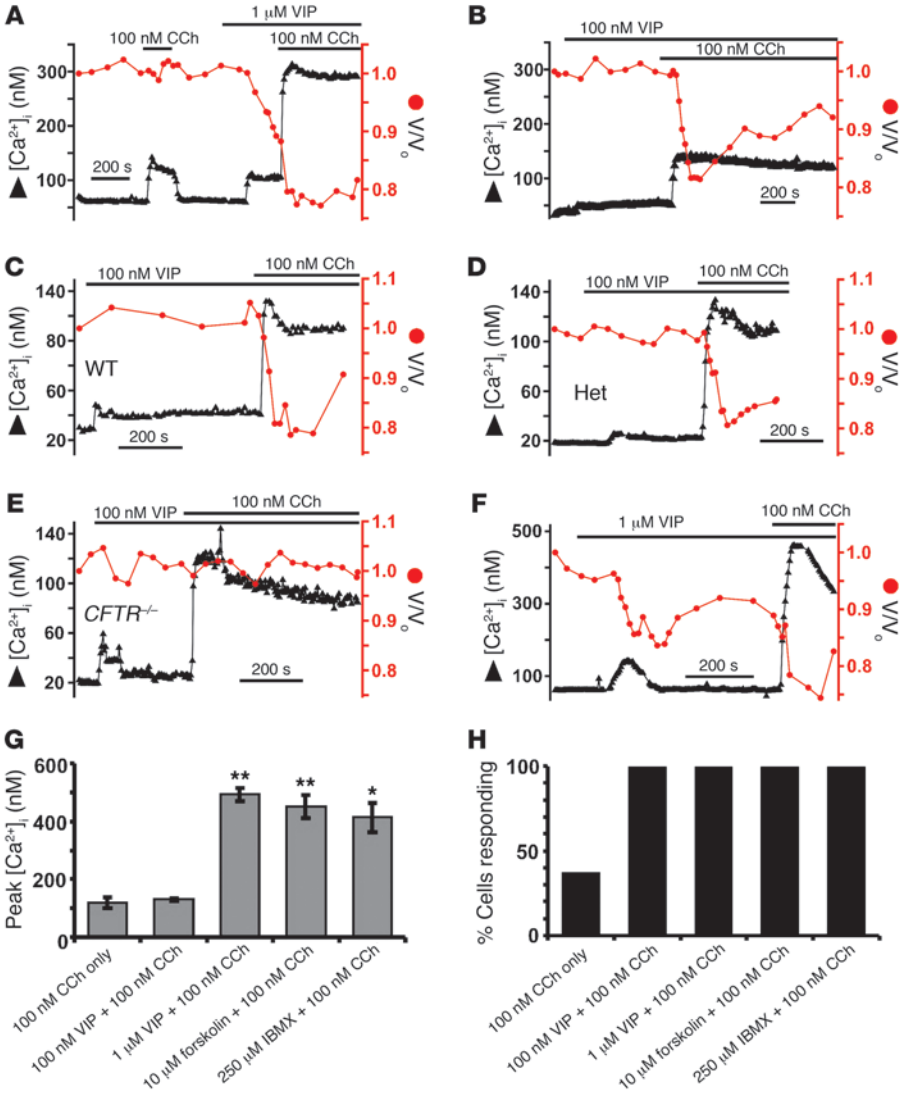

Figure 4

VIP potentiates low [CCh]-evoked responses in porcine serous cells. (**A**) In 3 of 8 bronchial cells, 100 nM CCh elicited $[Ca^{2+}]_i$ responses similar in magnitude to those evoked by 1 μM VIP; however, only VIP elicited shrinkage. (**B**) 100 nM VIP elicited smaller $[Ca^{2+}]_i$ elevations but no shrinkage. Subsequent 100 nM CCh elicited Ca^{2+}-rise and shrinkage in 100% of cells. (**C**–**E**) Neonatal tracheal cells stimulated with 100 nM VIP plus 100 nM CCh exhibited $[Ca^{2+}]_i$ elevations and CFTR-dependent shrinkage. Resting $[Ca^{2+}]_i$ was 34 ± 2 nM (WT; n = 13), 30 ± 2 nM (Het; n = 12), and 30 ± 6 nM (*CFTR*$^{-/-}$; n = 7). 100 nM VIP caused $[Ca^{2+}]_i$ elevation of 50 ± 4 nM (WT), 45 ± 3 nM (Het), and 56 ± 16 nM (*CFTR*$^{-/-}$). 100 nM CCh (in continued presence of VIP) elicited peak $[Ca^{2+}]_i$ responses of 128 ± 6 nM (WT), 132 ± 77 nM (Het), and 130 ± 16 nM (*CFTR*$^{-/-}$). Plateau $[Ca^{2+}]_i$ was 97 ± 5 nM (WT), 96 ± 6 nM (Het), and 83 ± 8 nM (*CFTR*$^{-/-}$). WT and Het cells shrank; *CFTR*$^{-/-}$ cells did not. (**F**) After 1 μM VIP, 100 nM CCh elicited higher $[Ca^{2+}]_i$ peak (492 ± 24 nM) and enhanced shrinkage in all cells. (**G** and **H**). $[Ca^{2+}]_i$ responses during 100 nM CCh stimulation of WT bronchial serous cells ± cAMP agonists. Asterisks represent significance compared with 100 nM CCh alone (Dunnett's test, $^*P < 0.05$; $^{**}P < 0.01$).

The $[Ca^{2+}]_i$ and CFTR requirements for VIP-induced secretion are independent. Our results indicate that CFTR, as well as a cAMP-induced rise of $[Ca^{2+}]_i$, is required for VIP activation of serous cell fluid secretion. This suggests that CFTR functions as the apical membrane secretory Cl^- channel during cAMP-activated fluid secretion. To evaluate this, a NO_3^- substitution protocol (30) was used in cells loaded with the fluorescent halide indicator SPQ. SPQ is quenched by Cl^- but not by NO_3^-. Most anion channels, including CFTR (31) and CaCC (32), have similar Cl^- and NO_3^- permeabilities. Replacement of extracellular Cl^- with NO_3^- causes electroneutral exchange of cellular Cl^- for NO_3^-, resulting in an increase in SPQ fluorescence. The rate of fluorescence increase can be used as a measure of relative plasma membrane anion permeability.

SPQ-loaded serous cells were loaded with BAPTA and stimulated in 0-$Ca^{2+}{}_o$, conditions that eliminated the $[Ca^{2+}]_i$ signal and secretion (as in Figure 1F). Experiments were performed in the presence of bumetanide and absence of CO_2/HCO_3^- to eliminate NKCC- and AE-mediated Cl^- transport, respectively. In the absence of stimulation, introduction of NO_3^- slowly enhanced SPQ fluorescence (Figure 3, A and B), suggesting low resting anion permeability. VIP (1 μM; Figure 3, A and B) or forskolin (10 μM; Supplemental Figure 5) enhanced the rate of SPQ fluorescence change by 10-fold (rates summarized in Supplemental Figure 5). Thus, VIP/cAMP activates a plasma membrane anion permeability in the absence of a rise of $[Ca^{2+}]_i$. VIP-stimulated Cl^- permeability was strongly inhibited by GlyH-101 and $CFTR_{inh}172$ ($P < 0.01$; Figure 3B), but not by the CaCC inhibitor niflumic acid (NFA; Figure 3B) (32). This suggests that VIP activates a cAMP- and CFTR-dependent, Ca^{2+}-independent anion permeability. Similar experiments were performed using serous cells from transgenic piglets. Basal unstimulated Cl^- permeabilities (Figure 3, C–F) and resting $[Cl^-]_i$ (Supplemental Figure 6) were similar among WT, Het, and *CFTR*$^{-/-}$ cells. VIP (1 μM) enhanced plasma membrane Cl^- permeability approximately 10-fold in the WT cells (Figure 3C), as in bronchial cells from older animals (Figure 3, A and B). However, VIP-induced Cl^- permeability was somewhat reduced in Het cells (Figure 3, D and F) and absent in *CFTR*$^{-/-}$ cells (Figure 3, E and F). VIP-stimulated rates of $\Delta F/F_{t=0}$ were 0.030 ± 0.001 (WT, n = 16), 0.025 ± 0.003 (Het, n = 15; $P < 0.05$ compared with WT), and 0.003 ± 0.001 (*CFTR*$^{-/-}$, n = 15; $P < 0.01$ compared with WT) units × s^{-1}. Together, these data suggest the cAMP-activated Cl^- permeability underlying fluid secretion is independent of the induced $[Ca^{2+}]_i$ rise and is mediated solely by CFTR.

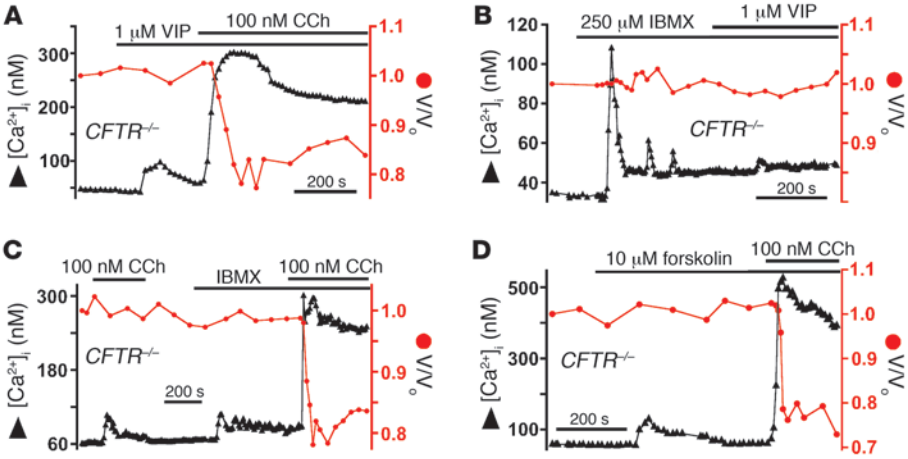

Figure 5
Strong cAMP stimulation restores low [CCh]-evoked secretion in *CFTR*$^{-/-}$ porcine tracheal gland serous cells. (**A**) In *CFTR*$^{-/-}$ cells, high [VIP] (1 μM) elicited exaggerated 100 nM CCh-stimulated $[Ca^{2+}]_i$ rise (340 ± 42 nM) correlated with shrinkage (19% ± 2%). (**B** and **C**) IBMX caused $[Ca^{2+}]_i$ elevation (104 ± 18 nM) but not shrinkage in *CFTR*$^{-/-}$ cells (n = 4). No additive effects were observed with VIP (**B**), but 100 nM CCh-evoked $[Ca^{2+}]_i$ responses were potentiated (303 ± 13 nM; n = 4; **C**), causing *CFTR*$^{-/-}$ cells to shrink (20% ± 2%). (**D**) Similar results observed with 10 μM forskolin pretreatment. Subsequent 100 nM CCh evoked-peak $[Ca^{2+}]_i$ response (455 ± 30 nM) was correlated with shrinkage (22% ± 2%; n = 5).

Low [VIP] potentiates CFTR-dependent Cl⁻ secretion responses to low [CCh]. Our results indicate that VIP/cAMP-activated serous cell fluid secretion requires both CFTR and a rise of $[Ca^{2+}]_i$, but the $[Ca^{2+}]_i$ signal is not required for CFTR activation. What is the role of the cAMP-induced rise of $[Ca^{2+}]_i$? Low-level cholinergic stimulation (100 nM CCh) elevated $[Ca^{2+}]_i$ to 120 ± 18 nM in only some (approximately 40%) cells (Figure 4A), as observed previously (4). This $[Ca^{2+}]_i$ elevation is of similar magnitude to that elicited by VIP, but in contrast to VIP, it was insufficient to stimulate secretion (Figure 4A). 100 nM CCh failed to enhance plasma membrane Cl^- permeability in any of 40 serous cells and acini examined (Supplemental Figure 5, J–K). Thus, the $[Ca^{2+}]_i$ elevation expected to occur in approximately 40% of these cells is insufficient to activate CaCC. Therefore, the Ca^{2+} dependence of cAMP-induced secretion involves CFTR-independent mechanisms having Ca^{2+} sensitivities higher than CaCC.

Lower [VIP] (100 nM) caused a small sustained elevation of $[Ca^{2+}]_i$ that failed to activate secretion (Figure 4B). However, subsequent addition of 100 nM CCh, itself also insufficient to stimulate secretion (Figure 4A), consistently induced robust shrinkage (14% ± 3%) in 100% of cells (n = 6; Figure 4B). Of interest, the peak $[Ca^{2+}]_i$ elicited by combined exposure to 100 nM VIP and 100 nM CCh (130 ± 5 nM; n = 6) was similar to that elicited by 100 nM CCh alone (Figure 4, A and G) and still smaller than that required to activate secretion with (higher concentrations of) CCh alone (3, 4). 100 nM VIP similarly enhanced the number of cells exhibiting $[Ca^{2+}]_i$ responses to 100 nM CCh in WT, Het, and *CFTR*$^{-/-}$ neonatal tracheal serous cells (Figure 4, C–E). Robust shrinkage was observed in WT (21% ± 1% within 50.4 ± 3 s; n = 10; Figure 4C) and Het cells (19% ± 2% within 67 ± 6 s; n = 12; magnitude NS but time P < 0.05 compared with WT; Figure 4D). In contrast, shrinkage was absent in *CFTR*$^{-/-}$ cells (Figure 4E). Thus, the synergistic secretory effects of 100 nM VIP plus 100 nM CCh require CFTR. As 100 nM VIP enhanced Cl^- permeability approximately 10-fold in WT cells (Supplemental Figure 5), low [VIP] likely enhances the secretory responses to low [CCh] by activating CFTR.

High [VIP] potentiates CFTR-independent Cl⁻ secretion responses to low [CCh]. The observations that CCh and VIP trigger Ca^{2+} release from the same internal stores and that low [VIP] enhanced the percentage of cells responding with $[Ca^{2+}]_i$ signals to low [CCh] suggested that cAMP can potentiate $InsP_3$-mediated Ca^{2+} release. In agreement, with cells preexposed to higher VIP (1 μM; Figure 4F), 100 nM CCh elicited markedly exaggerated $[Ca^{2+}]_i$ responses (492 ± 24 nM) in 100% of cells (n = 10) compared with either no preexposure (Figure 4A) or exposure to 100 nM VIP (Figure 4, B, G, and H). These exaggerated $[Ca^{2+}]_i$ signals resulted in more robust shrinkage than elicited by VIP alone (Figure 4F). The synergistic effects of 1 μM VIP on 100 nM CCh-evoked $[Ca^{2+}]_i$ responses were observed regardless of whether $[Ca^{2+}]_i$ remained elevated (Figure 4A) or had relaxed (Figure 4F). Similarly, pretreatment with 10 μM forskolin or 250 μM IBMX caused robust 100 nM CCh-stimulated $[Ca^{2+}]_i$ elevations of 450 ± 40 nM (n = 5) and 413 ± 50 nM (n = 4), respectively (both values NS compared with each other or 1 μM VIP plus 100 nM CCh; both values P < 0.01 compared with 100 nM CCh alone or 100 nM CCh plus 100 nM VIP) in 100% of cells (summarized in Figure 4, G and H). Thus, elevated $[cAMP]_i$ functionally sensitizes Ca^{2+} release to low [CCh], resulting in enhanced $[Ca^{2+}]_i$ signals. Are the enhanced $[Ca^{2+}]_i$ signals sufficient to activate CaCC? This was tested using *CFTR*$^{-/-}$ cells. Whereas neither VIP nor 100 nM CCh were able to elicit secrtion from *CFTR*$^{-/-}$ cells, 100 nM CCh activated robust secretion in *CFTR*$^{-/-}$ cells that were preexposed to 1 μM VIP (Figure 5A), 250 μM IBMX (Figure 5C), or 10 μM forskolin (Figure 5D).

Human nasal serous cells exhibit VIP-evoked cAMP- and Ca^{2+}-dependent cell shrinkage requiring Ca^{2+}-independent activation of CFTR. To determine whether the results obtained from the porcine models are relevant for human submucosal gland physiology, we isolated serous acinar cells from nasal turbinates obtained from non-CF individuals. The inferior nasal turbinates are rich in submucosal glands, which secrete copious amounts of fluid and mucus to humidify inspired air and trap particles and pathogens. Functional and histological studies have not revealed any significant differences between nasal submucosal glands and those found in lower airways (16, 33–37), and intact human nasal glands also exhibit CFTR-dependent fluid secretion in response to $[cAMP]_i$-elevating agonists (16, 37).

Human nasal serous acinar cells exhibited highly similar secretory responses to 1 μM VIP compared with porcine cells (Figure 6A). Resting $[Ca^{2+}]_i$ was 46 ± 3 nM (n = 67) in human serous cells. Upon 1 μM VIP stimulation, cells exhibited a $[Ca^{2+}]_i$ elevation (129 ± 6 nM; n = 8) that was temporally correlated with shrinkage (16% ± 1% within 90 ± 10 s; n = 8). Because agonist-induced cell shrinkage reflects loss of cell solute content upon activation of secretion in

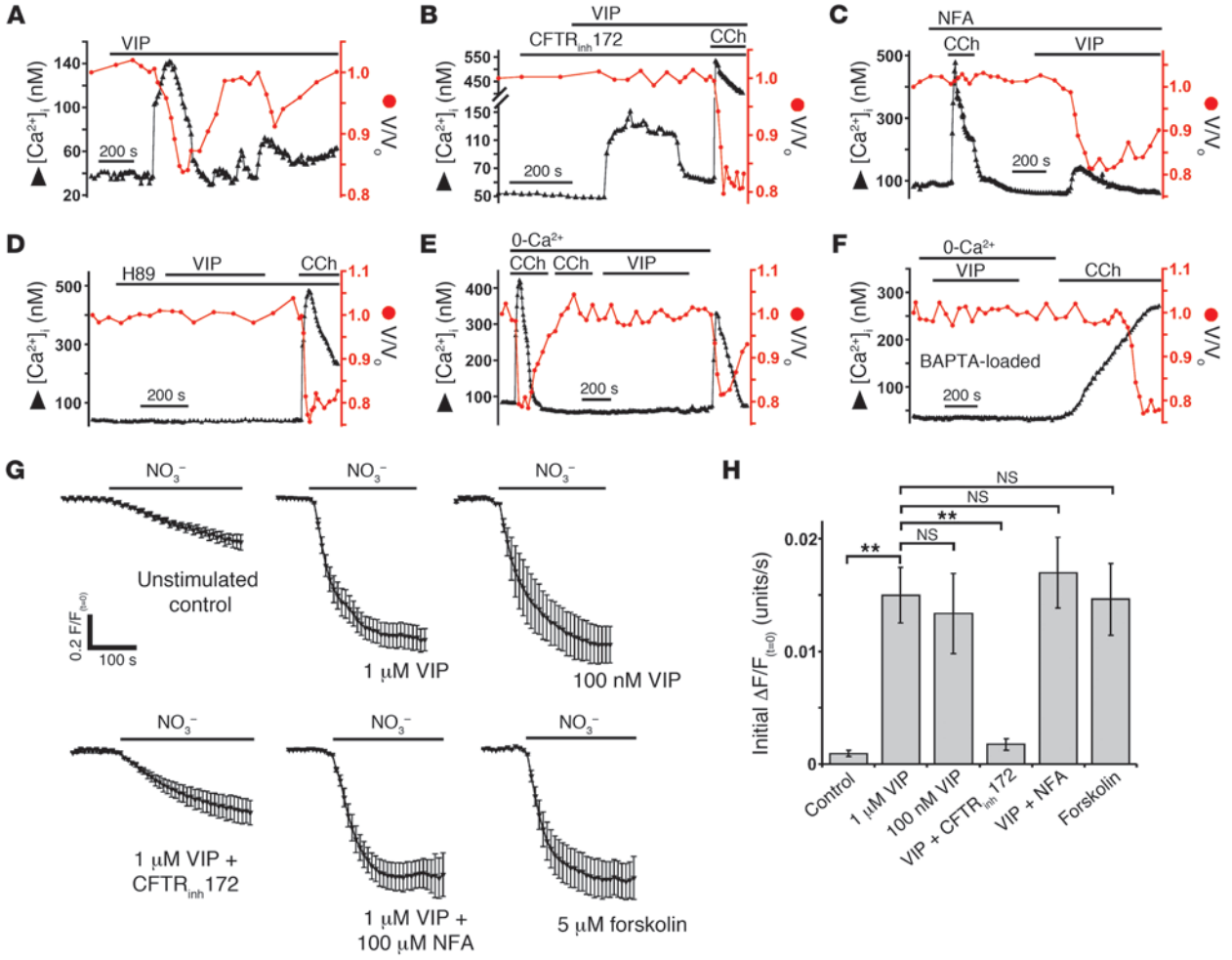

Figure 6

VIP stimulation of human nasal gland serous cell secretion requires both PKA-dependent Ca^{2+} signaling and Ca^{2+}-independent CFTR activation. (**A**) VIP (1 μM) caused cell shrinkage that was temporally correlated with elevation of $[Ca^{2+}]_i$. (**B** and **C**) VIP-activated shrinkage was completely blocked by $CFTR_{inh}172$ (12 μM, **B**); CCh-activated shrinkage was inhibited by NFA (150 μM, **C**). (**D**) VIP-activated $[Ca^{2+}]_i$ elevation and shrinkage were both abolished by H89 (10 μM). (**E**) After intracellular Ca^{2+} store depletion by stimulation with 100 μM CCh in 0-Ca^{2+}_o, subsequent stimulation with 1 μM VIP in 0-Ca^{2+}_o elicited neither $[Ca^{2+}]_i$ nor shrinkage responses. Reintroduction of Ca^{2+}_o caused a transient $[Ca^{2+}]_i$ elevation and shrinkage. (**F**) BAPTA-loading inhibited $[Ca^{2+}]_i$ elevation and shrinkage during stimulation with VIP in 0-Ca^{2+}_o. Reintroduction of Ca^{2+}_o in the presence of CCh caused a gradual rise of $[Ca^{2+}]_i$, activating shrinkage. (**G**) NO_3^- substitution was performed in BAPTA- and SPQ-loaded cells under 0-Ca^{2+}_o/0-$HCO_3^-{}_o$/100 μM bumetanide conditions (identical to Figure 3). VIP (100 nM and 1 μM) activated an approximately 15-fold increase in anion permeability that was mimicked by 5 μM forskolin and inhibited by 12 μM $CFTR_{inh}172$ but not by 150 μM NFA. Average traces shown (plotted inversely: downward deflection = increase in fluorescence = decrease in $[Cl^-]_i$) (**H**) Summary of initial rates of SPQ $\Delta F/F_{(t=0)}$ (units × s^{-1}) upon introduction of NO_3^-. ***P* < 0.01.

both murine (3, 17) and porcine (ref. 4 and this study) cells, it is very likely that VIP-evoked human serous cell shrinkage reflects activation of CFTR-dependent Cl^- secretion. In agreement, VIP-evoked shrinkage was completely blocked by $CFTR_{inh}172$ (Figure 6B; $n = 6$) but not by NFA (Figure 6C; 17% ± 2% shrinkage within 95 ± 10 s; $n = 7$), despite identical $[Ca^{2+}]_i$ responses (137 ± 9 nM and 132 ± 8 nM in the presence of $CFTR_{inh}172$ and NFA, respectively; both values NS compared with 1 μM VIP only). In contrast, NFA inhibited the shrinkage evoked by high $[Ca^{2+}]_i$ elevations during stimulation with 10 μM CCh (Figure 6C) while $CFTR_{inh}172$ did not. These results demonstrate that, as in porcine serous cells, 2 separate and parallel Cl^- secretion pathways exist in individual human serous cells: one mediated by CFTR and one mediated by CaCC.

Both VIP-evoked $[Ca^{2+}]_i$ elevation and CFTR-dependent shrinkage were inhibited by H89, suggesting that both responses are downstream of PKA (Figure 6D). Inhibition of the cAMP-dependent $[Ca^{2+}]_i$ response by depletion of Ca^{2+} stores (Figure 6E) or BAPTA buffering (Figure 6F) each eliminated VIP-evoked shrinkage in human cells. Taken together, these data suggest that human serous cell shrinkage is caused by KCl efflux through CFTR and Ca^{2+}-activated K^+ channels, as in porcine cells. To more directly determine whether the requirement for Ca^{2+} was independent of that for activation of CFTR, we performed NO_3^- substitution experiments to examine VIP-evoked changes in anion permeability under Ca^{2+}-buffered conditions, exactly as described for porcine cells (Figure 3). Average traces from independent experiments

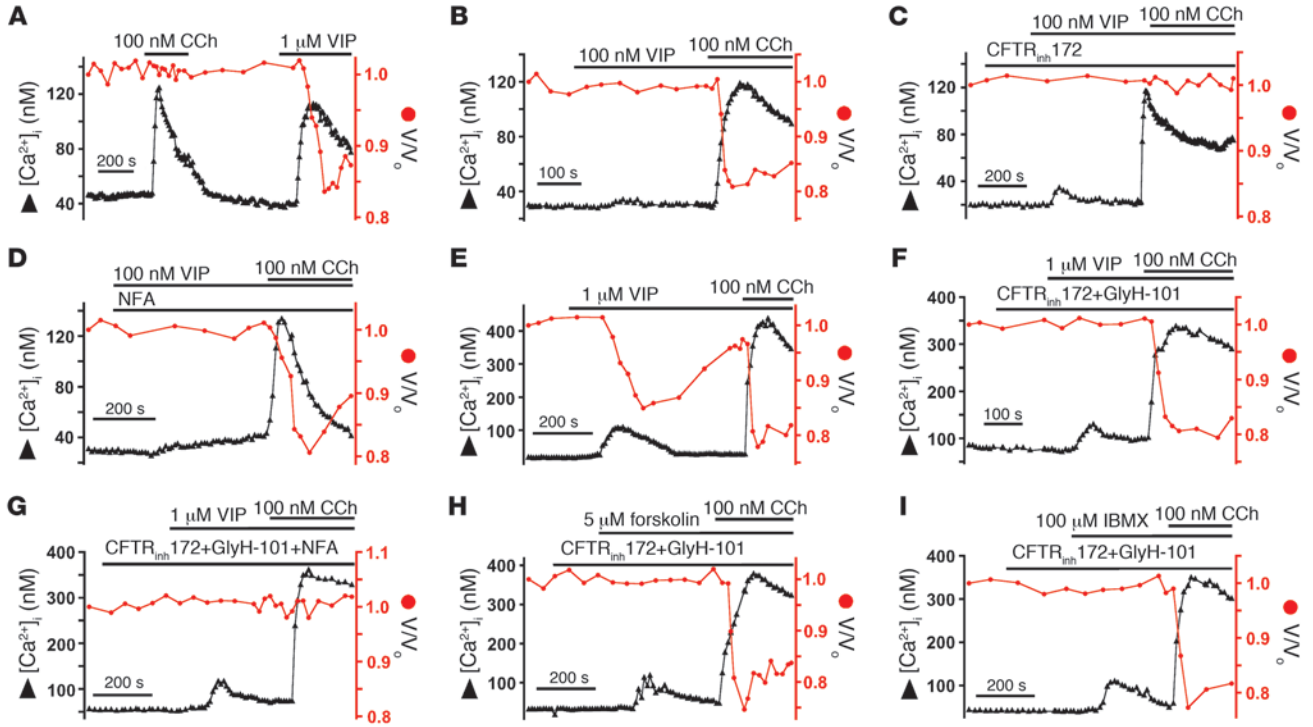

Figure 7
Human nasal gland serous acinar cells exhibit dose-dependent synergy between VIP and low-level cholinergic stimulation. (**A**) Stimulation with either 100 nM CCh or 1 μM VIP caused comparable $[Ca^{2+}]_i$ elevations in human serous cells, but only VIP caused cell shrinkage. (**B**) While a lower [VIP] (100 nM) had minimal effect on $[Ca^{2+}]_i$ and no effect on volume, it synergistically activated shrinkage in response to 100 nM CCh despite having no significant effect on the $[Ca^{2+}]_i$ response. (**C** and **D**) Shrinkage in response to 100 nm VIP + 100 nM CCh was inhibited by 12 μM $CFTR_{inh}172$ (**C**) but not by 150 μM NFA (**D**). (**E**–**G**). Higher [VIP] (1 μM) markedly potentiated the $[Ca^{2+}]_i$ elevation in response to 100 nM CCh (**E**), activating shrinkage that was insensitive to the presence of 12 μM $CFTR_{inh}172$ plus 5 μM GlyH-101 (**F**) but was blocked by NFA (**G**). (**H** and **I**) Strong cAMP stimulation with 5 μM forskolin (**H**) or 100 μM IBMX (**I**) likewise potentiated 100 nM CCh-evoked $[Ca^{2+}]_i$ responses, activating CFTR-independent shrinkage.

are shown in Figure 6G. Upon NO_3^- substitution, SPQ fluorescence increased by 0.001 $\Delta F/F_{(t=0)}$ units × s^{-1} in unstimulated (control) cells (n = 11). This rate was increased 15-fold by 1 μM VIP (0.015 ± 0.002 units × s^{-1}; n = 9; $P < 0.01$ compared with control by Dunnett's test), 100 nM VIP (0.013 ± 0.004 units × s^{-1}; n = 7; $P < 0.01$ compared with control by Dunnett's test; NS compared with 1 μM VIP), or 10 μM forskolin (0.015 ± 0.003 units × s^{-1}; n = 7; $P < 0.01$ compared with control by Dunnett's test; NS compared with 1 μM or 100 nM VIP). $CFTR_{inh}172$, which inhibited VIP-evoked shrinkage, markedly reduced the VIP-activated rate of SPQ unquenching upon NO_3^- substitution (0.0018 ± 0003 units × s^{-1}; n = 10; $P < 0.01$ compared with 1 μM or 100 nM VIP; $P < 0.05$ compared with control cells by Dunnett's test). In contrast, NFA had no significant effect ($\Delta F/F_{(t=0)}$ = 0.017 ± 0.003, n = 11; NS compared with 1 μM or 100 nM VIP; $P < 0.01$ compared with control by Dunnett's test). These data (summarized in Figure 6H) demonstrate that VIP activates a cAMP- and CFTR-dependent, Ca^{2+}-independent plasma membrane anion permeability, similar to that observed in porcine serous cells. Accordingly, the dependence of shrinkage on VIP-induced Ca^{2+} signaling is likely due to a requirement for activation of Ca^{2+}-activated K^+ permeabilities.

Strong cAMP stimulation can elicit CFTR-independent fluid secretion in response to low [CCh] due to potentiation of $[Ca^{2+}]_i$ responses and activation of CaCC. Because $[cAMP]_i$ elevation generated de novo PKA-dependent $[Ca^{2+}]_i$ responses in both porcine and human serous cells, we hypothesized that synergistic crosstalk between Ca^{2+} and cAMP is also likely present in both porcine and human cells. In human serous cells, low [CCh] (100 nM) elicited peak $[Ca^{2+}]_i$ responses (130 ± 5 nM in 100% of cells; n = 6; Figure 7A) that were similar in magnitude to those evoked by 1 μM VIP yet, unlike VIP, were nonetheless insufficient to activate secretion (Figure 6). However, after exposure to low [VIP] (100 nM, which had minimal effects on $[Ca^{2+}]_i$ and no effect on cell volume), 100 nM CCh evoked significant shrinkage (16% ± 2% within 85 ± 6 s in 100% of cells; n = 7; Figure 7B), despite no potentiation of the $[Ca^{2+}]_i$ response (128 ± 8 nM; NS compared with 100 nM CCh alone). This shrinkage was completely inhibited by $CFTR_{inh}172$ (Figure 7C; n = 6) despite identical $[Ca^{2+}]_i$ responses (125 ± 5 nM). In contrast, neither shrinkage (17% ± 1% within 88 ± 10 s) nor peak $[Ca^{2+}]_i$ (132 ± 8 nM) were affected by NFA (Figure 7D; n = 5; both values NS compared with 100 nM VIP plus 100 nM CCh). These data suggest that the mechanisms of CFTR-dependent synergy between low [VIP] and weak cholinergic stimulation observed in porcine serous cells (Figure 4) are present similarly in human serous cells.

To determine whether strong cAMP stimulation enables low-level cholinergic stimulation to evoke CFTR-independent secretion, as in the porcine cells, human cells were exposed to a higher [VIP] (1 μM) before stimulation with 100 nM CCh. CCh-evoked

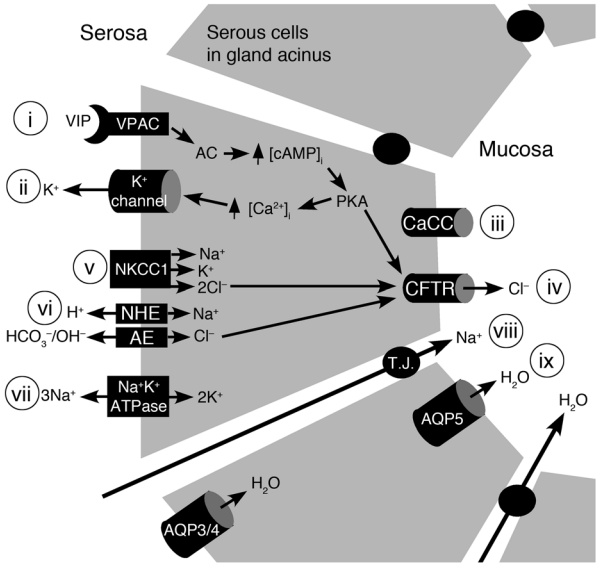

Figure 8
Model of VIP/cAMP evoked fluid secretion in porcine and human airway gland serous acinar cells. Binding of VIP to VPAC receptors (i) activates adenylyl cyclase–mediated (AC-mediated) elevation of $[cAMP]_i$, causing PKA-stimulated elevation of $[Ca^{2+}]_i$ required for activation of basolateral K^+ channels (ii). This $[Ca^{2+}]_i$ response is insufficient to activate CaCCs (iii). Thus, Cl^- secretion requires PKA-dependent activation of CFTR (iv). As during cholinergic stimulation, transepithelial Cl^- secretion is sustained by NKCC1 (v) and NHE/AE (vi), expressed on the basolateral membrane (4) and driven by Na^+ gradient established by the Na^+/K^+ ATPase (vii). While AE function was not elucidated directly in this study, canonical models of epithelial Cl^- secretion (reviewed in ref. 44) dictate that NHE-mediated alkalinization drives Cl^-/HCO_3^- exchange resulting in Cl^- uptake to sustain secretion. Secretion of Cl^- drives movement of Na^+ through a paracellular (tight junction; T.J.) pathway (viii) drawing osmotically obliged water into the gland lumen (ix) paracellularly or transcellularly through aquaporins (AQP; localization based on ref. 45). Our data suggest that activation of CaCC(s), either directly or indirectly through agents that enhance cAMP-activated $[Ca^{2+}]_i$ signals, could restore fluid secretion in serous cells lacking functional CFTR.

$[Ca^{2+}]_i$ and shrinkage were both markedly enhanced (Figure 7E; peak $[Ca^{2+}]_i$ = 358 ± 20 nM; n = 5). Neither the shrinkage nor $[Ca^{2+}]_i$ responses to 100 nM CCh after 1 μM VIP stimulation were inhibited by $CFTR_{inh}$172 and GlyH-101 (21% ± 2% shrinkage within 56 ± 7 s; peak $[Ca^{2+}]_i$ = 349 ± 21 nM; Figure 7F). However, shrinkage was completely abolished by NFA (Figure 7G) despite an identical peak Ca^{2+} response (356 ± 20 nM; n = 5). Stimulation with 5 μM forskolin (Figure 7H; n = 4) or 100 μM IMBX (Figure 7I; n = 5) likewise potentiated 100 nM CCh-evoked $[Ca^{2+}]_i$ responses (346 ± 12 nM and 325 ± 18 nM, respectively; NS) and activated robust CFTR-independent shrinkage (20% ± 2% within 62 ± 14 s and 20% ± 1% within 58 ± 9 s, respectively; NS compared with each other or with 1 μM VIP plus 100 nM CCh in the presence of $CFTR_{inh}$172 plus GlyH-101). These results suggest that porcine and human serous cells share similar mechanisms of Ca^{2+}-dependent CFTR-independent synergistic secretion during strong cAMP stimulation and low-level cholinergic stimulation.

Discussion

Here we have isolated primary serous acinar cells from porcine lung and human nasal turbinates to identify the mechanisms and regulation of cAMP-mediated fluid secretion, exploiting the availability of *CFTR*$^{-/-}$ pigs and pharmacological inhibitors to evaluate the role of CFTR. Porcine and human serous cells secrete fluid in response to VIP and other agents that raise $[cAMP]_i$ by mechanisms requiring CFTR and, unexpectedly, also a rise of $[Ca^{2+}]_i$ (summarized in Figure 8). The cAMP-mediated $[Ca^{2+}]_i$ signals involve release from $InsP_3$-sensitive Ca^{2+} stores that are shared by cAMP-independent agonists including cholinergic, histaminergic, and purinergic agonists that stimulate CFTR-independent secretion (4). The shared $[Ca^{2+}]_i$ signaling mechanisms between these distinct pathways provide 2 types of synergisms that strongly potentiate cAMP-mediated fluid secretion but differ in their CFTR dependencies. First, CFTR-dependent secretion is markedly potentiated by low VIP and CCh concentrations that individually are unable to stimulate secretion. Second, a higher [VIP] more strongly potentiates secretion by a low [CCh] that is unable to activate secretion alone. Importantly, this cAMP-potentiated secretion is CFTR independent, which therefore suggests novel therapeutic approaches for CF. Additionally, our data demonstrate that the mechanisms of fluid secretion and the role of CFTR in porcine and human serous cells are very similar, suggesting that WT and *CFTR*$^{-/-}$ pigs are a physiologically relevant model in which to study CFTR-dependent airway fluid secretion.

VIP activates cAMP-dependent Cl^- efflux through CFTR. Exposure of serous cells to VIP caused marked changes in cell volume. Similar responses were elicited by direct cAMP elevation (forskolin, IBMX) and inhibited by H89, suggesting that they are downstream of cAMP and PKA. As shown previously during CCh stimulation (3, 4), these cell volume changes track changes in solute content associated with activities of transport mechanisms involved in fluid secretion. First, these volume changes were associated with parallel changes in $[Cl^-]_i$. Second, shrinkage was inhibited by CFTR inhibitors and was absent in *CFTR*$^{-/-}$ cells. Third, swelling of porcine cells was inhibited by blockers of Na^+-dependent Cl^- influx pathways. Thus, VIP-induced shrinkage and swelling reflect solute efflux and influx, respectively. The observed approximate 15% shrinkage reflects an approximately 21% decrease in osmotically active cell volume (3, 4, 38). Using the relationship between $[Cl^-]_i$ and serous cell volume (Figure 1C), $[Cl^-]_i$ falls from approximately 65 mM at rest to approximately 39 mM at peak shrinkage, reflecting a loss of approximately 32 meq/l cellular Cl^- content. Assuming equal counter-ion (K^+) efflux, approximately 64 meq of cell solute content is lost, in good agreement with approximately 63 meq expected for 21% shrinkage of osmotically active volume in 300 mOsm medium. Because VIP-stimulated Cl^- efflux is completely CFTR dependent and CFTR is apically localized (Figure 2 and ref. 4), the Cl^- loss during shrinkage reflects Cl^- secretion through CFTR. The counter-ion K^+ efflux was not localized here, but must occur across the basolateral membrane through mechanisms remaining to be identified. Inhibition of swelling by bumetanide and DMA suggests that Cl^- uptake is mediated by both NKCC1 and paired NHE/AE activity located on the basolateral membrane, similar to the mechanism proposed for CCh-evoked secretion (4). Together, activities of these pathways constitute a mechanism for fluid secretion, and cell volume changes reflect the secretory activities of these cells (3, 4, 38).

The absence of cAMP-evoked secretion from *CFTR*$^{-/-}$ porcine serous cells and the GlyH-101 and $CFTR_{inh}172$ sensitivities of cAMP-evoked secretion in WT porcine and human cells demonstrate that cAMP-induced serous cell secretion is CFTR dependent, in agreement with results obtained from intact glands (5, 6, 8, 39). Despite the complexity of glands containing multiple cell types, the concordant results suggest that the serous cell mechanisms defined here contribute predominantly to the intact gland responses. In contrast, CCh-evoked secretion from WT (4) and *CFTR*$^{-/-}$ (this study) porcine serous cells, human nasal serous cells, and from intact glands (8, 40) is largely CFTR independent and inhibited by NFA. It has been speculated that CCh/Ca^{2+}-evoked and VIP/cAMP-evoked fluid secretion may originate from separate populations of gland cells (9), but our results demonstrate that 2 separate secretion pathways exist in the same serous cells, mediated by either CFTR or CaCC.

VIP activates cAMP-dependent $[Ca^{2+}]_i$ signaling. An unexpected finding was that VIP caused a cAMP-dependent $[Ca^{2+}]_i$ elevation that occurred concomitantly with and was required for KCl efflux. $[Ca^{2+}]_i$ elevation was caused by Ca^{2+} release from the same $InsP_3$-sensitive intracellular stores involved in CCh-stimulated Ca^{2+} release. Direct crosstalk between cAMP and Ca^{2+} signaling pathways has not been previously considered in serous acinar cells. The mechanisms accounting for cAMP activation of Ca^{2+} signals in serous cells remain to be established, although the substantial dose-dependent potentiation by cAMP of 100 nM CCh-evoked $[Ca^{2+}]_i$ signals suggests that cAMP likely enhances the $InsP_3$ sensitivity of the $InsP_3$ receptor ($InsP_3R$) (41). PKA phosphorylation of resident $InsP_3Rs$ could sensitize them to the basal $[InsP_3]_i$, generating a Ca^{2+} response in the absence of de novo $InsP_3$ production, and also augment $InsP_3R$ sensitivity to low $[InsP_3]_i$ produced during 100 nM CCh stimulation. While the predominant $InsP_3R$ isoform or isoforms in serous cells are unknown, all 3 isoforms can be phosphorylated by PKA in intact cells (41). Further work is required to identify the molecular mechanisms of crosstalk between Ca^{2+} and cAMP signaling in these cells.

An important yet surprising observation was that these Ca^{2+} signals were required for cAMP-activated secretion. While the Ca^{2+}-mobilizing agonist CCh has been shown to influence VIP-induced CFTR-dependent secretion (18), a direct requirement for $[Ca^{2+}]_i$ signaling during VIP-evoked secretion has not been previously demonstrated. The $[Ca^{2+}]_i$ signal is not required for activation of the anion permeability, since cAMP-induced secretion was completely dependent on CFTR and cAMP still activated CFTR Cl^- permeability in cells lacking the $[Ca^{2+}]_i$ signal. The simplest explanation is that cAMP activates CFTR to serve as the secretory Cl^- channel, while the cAMP-induced $[Ca^{2+}]_i$ rise is required for activation of K^+ channels to mediate counter-ion efflux. Accordingly, resting K^+ conductance must be unexpectedly small and fundamentally limiting when cAMP is raised in the absence of a concomitant rise of $[Ca^{2+}]_i$. This can account for the temporal correlation between the cAMP-induced rise of $[Ca^{2+}]_i$ and initiation of shrinkage, despite variable latencies of the $[Ca^{2+}]_i$ responses. Despite a modest reduction in Cl^- permeability in Het serous cells, 1 μM VIP or 10 μM forskolin-evoked shrinkage was identical in Het and WT cells, suggesting that K^+ conductance remains rate limiting even during secretion evoked by strong cAMP stimulation. The serous cells must also have very low resting Cl^- conductance. Thus, 100 nM CCh or 1 μM VIP elicited comparable $[Ca^{2+}]_i$ elevations that are sufficient to activate the K^+ conductance (since VIP elicited KCl efflux), but 100 nM CCh failed to induce shrinkage, indicating that resting Cl^- conductance was very small and the small $[Ca^{2+}]_i$ elevation was insufficient to activate CaCC. Insensitivity of VIP/forskolin-activated Cl^- efflux to NFA also indicates that the magnitude of the VIP-induced $[Ca^{2+}]_i$ signal is insufficient to activate CaCC (4).

Synergism between cAMP and cholinergic activated secretion mediated by CFTR-dependent and -independent mechanisms. We found potent synergisms between VIP and cholinergic stimulation. Concentrations of CCh and VIP that were insufficient to activate secretion when applied alone induced robust secretion when added together. Similar synergism between VIP and CCh has been observed in intact human and porcine submucosal glands (18) and may have important implications for airway physiology (11). However, our studies provide what we believe are novel insights into the cellular mechanisms of this synergism by suggesting that it resides in the ability of VIP to potentiate CCh-induced $InsP_3$-mediated Ca^{2+} release. 100 nM VIP was as potent as 1 μM VIP in activating CFTR, but it failed to induce secretion, indicating that the $[Ca^{2+}]_i$ elevation produced was insufficient to activate K^+ conductance. However, low [VIP] enabled low [CCh] to raise $[Ca^{2+}]_i$ sufficiently to activate K^+ conductance in all cells, resulting in a synergistic activation of CFTR-dependent secretion. Of note, these results suggest that cAMP-activated K^+ conductances play little role in secretion, in contrast with speculations (18). Higher [VIP] more strongly potentiated the low [CCh]-evoked $[Ca^{2+}]_i$ to levels that were sufficient to activate the CaCC in addition to the K^+ conductance, resulting in cAMP-dependent secretion in CFTR-deficient cells.

Together, our results suggest that VIP activates fluid secretion by 2 cAMP-dependent mechanisms operating in parallel: activation of CFTR as a secretory Cl^- channel and mobilization of Ca^{2+} from $InsP_3$-sensitive stores. The released Ca^{2+} activates counter-ion K^+ channels, resulting in KCl efflux and cell shrinkage. Low [VIP] cannot activate secretion because it does not raise $[Ca^{2+}]_i$ high enough to activate K^+ channels and cAMP cannot activate them either. Alternately, low [CCh] is unable to activate secretion because it does not raise $[Ca^{2+}]_i$ sufficiently to activate CaCC and it cannot activate CFTR. Low concentrations of both agonists synergize to activate secretion because VIP can activate CFTR and it enables CCh to raise $[Ca^{2+}]_i$ sufficiently to activate K^+ conductances. High [CCh] activates secretion by elevating $[Ca^{2+}]_i$ sufficiently to activate both K^+ channels and CaCC, bypassing the requirement for CFTR. Importantly, high $[cAMP]_i$ enables low [CCh] to activate CFTR-independent secretion by strongly potentiating CCh-induced $[Ca^{2+}]_i$ signals to levels that activate CaCC.

Implications for CF. Insufficient submucosal gland fluid secretion may contribute to airway dehydration and CF pathophysiology (9). Our results indicate that serous acinar cells secrete fluid by either CFTR- or CaCC-dependent mechanisms. The presence of both mechanisms in the same cells suggests that CaCC could be targeted therapeutically to compensate for lack of CFTR function in CF cells. A general problem in considering alternative channels is that they are often regulated by distinct signal transduction mechanisms, i.e., signals that activate CFTR do not activate CaCC. Therapeutic strategies targeting CaCC must therefore impinge on those signaling pathways that activate CaCC. However, this would not necessarily stimulate secretion at appropriate times in a physiological context. A preferable approach would be to exploit the signal transduction mechanisms generated in vivo at physiologically appropriate times that normally activate CFTR. Here, we have

demonstrated crosstalk between the cAMP pathway that activates CFTR and the Ca^{2+} pathway that activates CaCC. This crosstalk affords new therapeutic strategies. For example, a CaCC potentiator sensitizing it to lower $[Ca^{2+}]_i$ would enable CF serous cells to secrete in response to cAMP agonists. Agents that enhance the magnitude of the cAMP-stimulated $[Ca^{2+}]_i$ response (e.g., by elevating resting $[InsP_3]_i$ or sensitizing the $InsP_3R$ to $InsP_3$) might also enable cAMP agonists to activate CaCC-mediated secretion. cAMP-elevating drugs, e.g., phosphodiesterase inhibitors, could enable low-level cholinergic stimulation to activate CFTR-independent secretion. Importantly, such agents would lead to secretion only during times of physiological stimuli, utilizing the appropriate neural regulation of secretion that likely remains intact in CF.

It has been proposed that airway inflammation expands $InsP_3$-sensitive Ca^{2+} stores, leading to exaggerated Ca^{2+} release in response to $InsP_3$-generating agonists (42). We observed no enhancement of $InsP_3$-activated Ca^{2+} release in porcine *CFTR*$^{-/-}$ serous cells, but they were obtained from disease-free neonatal lungs. Ca^{2+} store expansion with CF disease progression could possibly result in enhanced Ca^{2+} release in response to low-level cholinergic stimulation that could activate CFTR-independent secretion. Furthermore, our results suggest that inflammatory mediators that elevate cAMP could enhance low-level cholinergic-evoked Ca^{2+} responses and promote CFTR-independent secretion. Whether such responses exist and whether they would be beneficial or exacerbate lung pathology are unknown. The lungs of *CFTR*$^{-/-}$ pigs spontaneously develop substantial CF-like airway inflammation and pathology over several months (29). It may therefore be possible to test these ideas in future studies.

Methods

Reagents and experimental solutions. VIP was obtained from Advanced ChemTech/CreoSalus or Sigma-Aldrich. Alexa Fluor (AF) secondary antibodies, fura-2-AM, SPQ, BAPTA-AM, and SNARF-5F-AM were purchased from Invitrogen. Collagenase and DNase I were obtained from Worthington Biochemical. Cell-Tak was purchased from BD Biosciences. Vectashield mounting medium was purchased from Vector Labs. All other reagents were from Sigma-Aldrich.

The primary extracellular solution (solution A) contained 125 mM NaCl, 5 mM KCl, 1.2 mM $MgCl_2$, 1.2 mM $CaCl_2$, 1.2 mM NaH_2PO_4, 11 mM glucose, and 25 mM $NaHCO_3^-$ buffered to pH 7.4 by 95% O_2/5% CO_2 gassing (3, 4, 17). Experiments performed in the absence of extracellular Ca^{2+} (0-$Ca^{2+}{}_o$) employed $CaCl_2$-free solution A plus 1 mM EGTA. Dissection of tissue and gland isolation (as described in ref. 4) utilized buffer lacking $NaHCO_3^-$ and containing 20 mM HEPES, 2 mM L-glutamine, 1× penicillin/streptomycin, 50 μg/ml gentamicin, and 1× MEM vitamins, amino acids, and nonessential amino acids (solution B). Tissue was transported to the lab at approximately 4°C in solution B plus 1 μM indomethacin (7). Overnight storage at 4°C employed solution B lacking indomethacin. Collagenase digestion utilized solution B with Ca^{2+} omitted. The control solution for NO_3^- substitution experiments (solution C; ref. 30) contained 136.2 mM NaCl, 3.8 mM KCl, 1.2 mM KH_2PO_4, 1.2 mM $CaCl_2$, 1.2 mM $MgCl_2$, 11 mM glucose, and 10 mM HEPES, pH 7.4 ($[Cl^-]_o$ = 144.8 mM), gassed with 100% O_2. The low $[Cl^-]_o$ solution (solution D) was identical to solution C except NaCl was replaced isosmotically with $NaNO_3$ ($[Cl^-]_o$ = 8.6 mM).

Isolation of porcine bronchial and tracheal submucosal gland serous acinar cells. Lung tissue was obtained from WT pigs (approximately 30–35 kg; *Sus scrofa domestica*) from mixed genetic backgrounds euthanized by KCl injection following unrelated procedures (ref. 4; provided by L.B. Becker and M. Boller, Department of Emergency Medicine, University of Pennsylvania) or from a local abattoir (Hatfield Quality Meats, Hatfield, Pennsylvania, USA) within 10 minutes after death. No differences were observed between cells isolated from either source. Neonatal porcine tracheae from pigs 24 to 48 hours old (n = 7 WT, 6 Het, and 5 *CFTR*$^{-/-}$) were provided by M.J. Welsh and P.H. Karp (University of Iowa, Iowa City, Iowa, USA). Whenever possible, *CFTR*$^{-/-}$ cells were compared directly with cells from WT and Het littermates. All procedures were approved by the University of Pennsylvania Institutional Animal Care and Use Committee. Serous cells were isolated by incubation of dissected submucosal glands in types 2 and 4 collagenases (1 mg × ml^{-1} each) and DNAse I (10 μg × ml^{-1}) for approximately 40 minutes at room temperature as described (4). After gentle centrifugation, cells were resuspended in either solution A or solution C, plated on Cell-Tak coated coverslips, and imaged within 6–8 hours after isolation.

Isolation of human nasal submucosal gland serous acinar cells. Human inferior turbinate was provided by N.A. Cohen, J.N. Palmer, A.G. Chiu, and D.W. Kennedy and L. Doghramji (Department of Otorhinolaryngology, University of Pennsylvania and Veterans Affairs Medical Center, Philadelphia, Pennsylvania, USA). Tissue was obtained with approval of the University of Pennsylvania Institutional Review Board and written consent from 9 non-CF adult patients undergoing turbinectomy procedures related to chronic sinusitis and/or allergic rhinitis. Tissue was transported to the lab in ice-cold PBS. Epithelium was cut from the bone in ice-cold solution B and either used directly or stored at 4°C as described above. The dense connective tissue underlying the turbinate epithelium necessitated a stronger digestion protocol. Gland-rich submucosal tissue was dissected away from surface epithelium and incubated for 1.5 hours in types 2 and 4 collagenases (2 mg × ml^{-1} each) and 10 μg × ml^{-1} DNase I. After washing, cells were plated on coverslips and imaged within approximately 6 hours. No detectable differences were observed in the responses of cells isolated from different individuals; all responses were very similar to those observed in porcine serous cells (this study and ref. 4). Nonetheless, all results were confirmed using at least 2 different cell preparations on separate days using tissue from different individuals.

Simultaneous DIC/fluorescence live cell imaging. Serous cells were loaded with fura-2 by incubation in 2 μM fura-2-AM for 10 minutes at room temperature. Cells were loaded with SPQ by approximately 1- to 2-hour incubation in 20 mM SPQ. Simultaneous DIC and fluorescence imaging of cells and small acini was performed as described (3, 38, 43). Cells were typically imaged immediately after loading, but loaded cells remained viable on coverslips for more than 45 minutes. Conversions of fura-2 340 nm/380 nm ratios to $[Ca^{2+}]_i$ and conversion of SPQ fluorescence changes to $[Cl^-]_i$ were performed as described (3, 4, 38). Relative cell/acini volume changes were determined by raising the DIC-imaged cross-sectional area to the 3/2 power (3, 4, 17, 38, 43). All experiments were performed at 37°C.

Confocal immunofluorescence microscopy. Immunocytochemistry was performed as described (3, 4, 17) using anti-CFTR mouse monoclonal antibody 24-1. Briefly, plated cells were fixed for 20 minutes in 4% formaldehyde in PBS (+Ca^{2+}, +Mg^{2+}) at room temperature. Permeabilization and primary antibody incubation were performed in PBS (+ 2% BSA, 2% goat serum, and 0.1% saponin) overnight at 4°C. Following washing, coverslips were incubated in PBS plus BSA/serum/saponin containing AF488-conjugated secondary antibody for 1–2 hours at 4°C. Coverslips were mounted using Vectashield mounting medium and imaged on an inverted Nikon microscope (×60, 1.4 NA objective) equipped with a PerkinElmer Ultraview confocal system. Identical microscope (objective, laser power) and camera (exposure, gain, binning) settings were used to image WT and *CFTR*$^{-/-}$ cells.

Software and statistical analysis. Images were acquired using Ultraview software (PerkinElmer). Data were analyzed using Excel (Microsoft), Igor Pro (WaveMetrics Inc.), and/or ImageJ (W. Rasband, NIH). Unless indicated, all

values are represented as mean ± SEM. Two-tailed Student's *t* test (Excel) was used to determine statistical significance (*P* value) unless indicated otherwise. When indicated, 2-tailed Dunnett's test (Igor Pro) was used. $P < 0.05$ was considered significant.

Acknowledgments

These studies were supported by a postdoctoral fellowship to R.J. Lee (LEE09F0) and a research grant to J.K. Foskett (FOSKET07G0), both from the CF Foundation. The authors would like to thank M. Welsh and P. Karp (supported by NIH grants HL51670 and HL91842 and the CF foundation) for providing transgenic *CFTR*$^{-/-}$ piglet tissue; M. Boller and L. Becker for providing adult WT pig tissue; and N.A. Cohen, J.N. Palmer, A.G. Chiu, D.W. Kennedy, and L. Doghramji for supplying human nasal tissue.

Received for publication March 15, 2010, and accepted in revised form June 1, 2010.

Address correspondence to: J. Kevin Foskett, Department of Physiology, B39 Anatomy-Chemistry Building, University of Pennsylvania, Philadelphia, Pennsylvania 19104-6085, USA. Phone: 215.898.1354; Fax: 215.573.6808; E-mail: foskett@mail.med.upenn.edu.

1. Ballard ST, Spadafora D. Fluid secretion by submucosal glands of the tracheobronchial airways. *Respir Physiol Neurobiol*. 2007;159(3):271–277.
2. Engelhardt JF, et al. Submucosal glands are the predominant site of CFTR expression in the human bronchus. *Nat Genet*. 1992;2(3):240–248.
3. Lee RJ, Limberis MP, Hennessy MF, Wilson JM, Foskett JK. Optical imaging of Ca^{2+}-evoked fluid secretion by murine nasal submucosal gland serous acinar cells. *J Physiol*. 2007;582(pt 3):1099–1124.
4. Lee RJ, Foskett JK. Mechanisms of Ca^{2+}-stimulated fluid secretion by porcine bronchial submucosal gland serous acinar cells. *Am J Physiol Lung Cell Mol Physiol*. 2010;298(2):L210–L231.
5. Joo NS, Irokawa T, Robbins RC, Wine JJ. Hyposecretion, not hyperabsorption, is the basic defect of cystic fibrosis airway glands. *J Biol Chem*. 2006; 281(11):7392–7398.
6. Joo NS, Irokawa T, Wu JV, Robbins RC, Whyte RI, Wine JJ. Absent secretion to vasoactive intestinal peptide in cystic fibrosis airway glands. *J Biol Chem*. 2002;277(52):50710–50715.
7. Joo NS, Saenz Y, Krouse ME, Wine JJ. Mucus secretion from single submucosal glands of pig. Stimulation by carbachol and vasoactive intestinal peptide. *J Biol Chem*. 2002;277(31):28167–28175.
8. Ianowski JP, Choi JY, Wine JJ, Hanrahan JW. Mucus secretion by single tracheal submucosal glands from normal and CFTR knock-out mice. *J Physiol*. 2007;580(pt 1):301–314
9. Wine JJ, Joo NS. Submucosal glands and airway defense. *Proc Am Thorac Soc*. 2004;1(1):47–53.
10. Dickson L, Finlayson K. VPAC and PAC receptors: From ligands to function. *Pharmacol Ther*. 2009;121(3):294–316.
11. Wine JJ. Parasympathetic control of airway submucosal glands: central reflexes and the airway intrinsic nervous system. *Auton Neurosci*. 2007;133(1):35–54.
12. Lazarus SC, Basbaum CB, Barnes PJ, Gold WM. cAMP immunocytochemistry provides evidence for functional VIP receptors in trachea. *Am J Physiol*. 1986;251(1 pt 1):C115–C119.
13. Peatfield AC, Barnes PJ, Bratcher C, Nadel JA, Davis B. Vasoactive intestinal peptide stimulates tracheal submucosal gland secretion in ferret. *Am Rev Respir Dis*. 1983;128(1):89–93.
14. Liu YC, Khawaja AM, Rogers DF. Effect of vasoactive intestinal peptide (VIP)-related peptides on cholinergic neurogenic and direct mucus secretion in ferret trachea in vitro. *Br J Pharmacol*. 1999; 128(6):1353–1359.
15. Wagner U, Bredenbroker D, Storm B, Tackenberg B, Fehmann HC, von Wichert P. Effects of VIP and related peptides on airway mucus secretion from isolated rat trachea. *Peptides*. 1998;19(2):241–245.
16. Salinas D, et al. Submucosal gland dysfunction as a primary defect in cystic fibrosis. *FASEB J*. 2005; 19(3):431–433.
17. Lee RJ, Harlow JM, Limberis MP, Wilson JM, Foskett JK. HCO_3^- secretion by murine nasal submucosal gland serous acinar cells during Ca^{2+}-stimulated fluid secretion. *J Gen Physiol*. 2008;132(1):161–183.
18. Choi JY, et al. Synergistic airway gland mucus secretion in response to vasoactive intestinal peptide and carbachol is lost in cystic fibrosis. *J Clin Invest*. 2007; 117(10):3118–3127.
19. Fatatis A, Holtzclaw LA, Avidor R, Brenneman DE, Russell JT. Vasoactive intestinal peptide increases intracellular calcium in astroglia: synergism with alpha-adrenergic receptors. *Proc Natl Acad Sci U S A*. 1994;91(6):2036–2040.
20. Schaad NC, Vanecek J, Rodriguez IR, Klein DC, Holtzclaw L, Russell JT. Vasoactive intestinal peptide elevates pinealocyte intracellular calcium concentrations by enhancing influx: evidence for involvement of a cyclic GMP-dependent mechanism. *Mol Pharmacol*. 1995;47(5):923–933.
21. Low AM, Sormaz L, Kwan CY, Daniel EE. Mobilization of internal Ca^{2+} by vasoactive intestinal polypeptide in endothelial cells. *Eur J Pharmacol*. 1997;339(2–3):227–235.
22. Langer I, Perret J, Vertongen P, Waelbroeck M, Robberecht P. Vasoactive intestinal peptide (VIP) stimulates $[Ca^{2+}]_i$ and cyclic AMP in CHO cells expressing Galpha16. *Cell Calcium*. 2001;30(4):229–234.
23. McCulloch DA, et al. Additional signals from VPAC/PAC family receptors. *Biochem Soc Trans*. 2002; 30(4):441–446.
24. Yamada H, Watanabe M, Yada T. Cytosolic Ca^{2+} responses to sub–picomolar and nanomolar PACAP in pancreatic beta–cells are mediated by VPAC2 and PAC1 receptors. *Regul Pept*. 2004;123(1–3):147–153.
25. Hagen BM, Bayguinov O, Sanders KM. VIP and PACAP regulate localized Ca^{2+} transients via cAMP-dependent mechanism. *Am J Physiol Cell Physiol*. 2006; 291(2):C375–C385.
26. Muanprasat C, Sonawane ND, Salinas D, Taddei A, Galietta LJ, Verkman AS. Discovery of glycine hydrazide pore-occluding CFTR inhibitors: mechanism, structure-activity analysis, and in vivo efficacy. *J Gen Physiol*. 2004;124(2):125–137.
27. Ma T, et al. Thiazolidinone CFTR inhibitor identified by high-throughput screening blocks cholera toxin-induced intestinal fluid secretion. *J Clin Invest*. 2002;110(11):1651–1658.
28. Rogers CS, et al. Disruption of the CFTR gene produces a model of cystic fibrosis in newborn pigs. *Science*. 2008;321(5897):1837–1841.
29. Stoltz DA, et al. Cystic fibrosis pigs develop lung disease and exhibit defective bacterial eradication at birth. *Sci Transl Med*. 2010;2(29):29ra31.
30. Dho S, Foskett JK. Optical imaging of Cl^- permeabilities in normal and CFTR-expressing mouse L cells. *Biochim Biophys Acta*. 1993;1152(1):83–90.
31. Dawson DC, Smith SS, Mansoura MK. CFTR: mechanism of anion conduction. *Physiol Rev*. 1997;79(1 suppl):S47–S75.
32. Hartzell C, Putzier I, Arreola J. Calcium-activated chloride channels. *Annu Rev Physiol*. 2005;67:719–758.
33. Raphael GD, Jeney EV, Baraniuk JN, Kim I, Meredith SD, Kaliner MA. Pathophysiology of rhinitis. Lactoferrin and lysozyme in nasal secretions. *J Clin Invest*. 1989;84(5):1528–1535.
34. Baraniuk JN, Kaliner MA. Neuropeptides and nasal secretion. *J Allergy Clin Immunol*. 1990; 86(4 pt 2):620–627.
35. Baraniuk JN, et al. Vasoactive intestinal peptide in human nasal mucosa. *J Clin Invest*. 1990; 86(3):825–831.
36. Groneberg DA, et al. Distribution of respiratory mucin proteins in human nasal mucosa. *Laryngoscope*. 2003;113(3):520–524.
37. Song Y, Salinas D, Nielson DW, Verkman AS. Hyperacidity of secreted fluid from submucosal glands in early cystic fibrosis. *Am J Physiol Cell Physiol*. 2005;290(3):C741–C749.
38. Foskett JK. $[Ca^{2+}]_i$ modulation of Cl^- content controls cell volume in single salivary acinar cells during fluid secretion. *Am J Physiol*. 1990; 259(6 pt 1):C998–C1004.
39. Thiagarajah JR, Song Y, Haggie PM, Verkman AS. A small molecule CFTR inhibitor produces cystic fibrosis-like submucosal gland fluid secretions in normal airways. *FASEB J*. 2004;18(7):875–877.
40. Choi JY, et al. Substance P stimulates human airway submucosal gland secretion mainly via a CFTR-dependent process. *J Clin Invest*. 2009;119(5):1189–1200.
41. Foskett JK, White C, Cheung KH, Mak DO. Inositol trisphosphate receptor Ca^{2+} release channels. *Physiol Rev*. 2007;87(2):593–658.
42. Ribeiro CM, Paradiso AM, Carew MA, Shears SB, Boucher RC. Cystic fibrosis airway epithelial $Ca^{2+}{}_i$ signaling: the mechanism for the larger agonist-mediated $Ca^{2+}{}_i$ signals in human cystic fibrosis airway epithelia. *J Biol Chem*. 2005;280(11):10202–10209.
43. Foskett JK, Melvin JE. Activation of salivary secretion: coupling of cell volume and $[Ca^{2+}]_i$ in single cells. *Science*. 1989;244(4912):1582–1585.
44. Melvin JE, Yule D, Shuttleworth T, Begenisich T. Regulation of fluid and electrolyte secretion in salivary gland acinar cells. *Annu Rev Physiol*. 2005;67:445–469.
45. Verkman AS, Matthay MA, Song Y. Aquaporin water channels and lung physiology. *Am J Physiol Lung Cell Mol Physiol*. 2000;278(5):L867–L879.